Mechanisms for magnetic-field generation in laser plasmas

V. Yu. Bychenkov, Yu. S. Kas'yanov,* G. S. Sarkisov, and V. T. Tikhonchuk

P. N. Lebedev Physics Institute, Russian Academy of Sciences, 117924 Moscow, Russia
**Institute of General Physics, Russian Academy of Sciences, 117924 Moscow, Russia*

(Submitted 8 July 1993)
Pis'ma Zh. Eksp. Teor. Fiz. **58**, No. 3, 183–188 (10 August 1993)

The spatial–temporal structure of magnetic fields in a laser plasma has been studied by a Faraday-effect method for the first time, at incident beam intensities $\sim 5\times 10^{14}$ W/cm^2. Analysis of the experimental data shows that the magnetic fields are generated as a result of the excitation of a thermal emf and a ponderomotive emf. The spatial structure of the magnetic field indicates that this field has an important effect on the hydrodynamics of the plasma corona.

Research on the space–time structure of magnetic fields and on mechanisms for generating these fields is of major interest for the problem of laser fusion. The primary reason is that megagauss-range magnetic fields can seriously limit the energy transfer from the region in which the laser light is absorbed to the evaporation zone at the target surface. They can also disrupt the uniformity of the heat transfer in the plasma corona. Most of the experiments in which megagauss-range magnetic fields have been detected[1–4] have focused on an analysis of the spatial structure of the magnetic field, basically ignoring the time evolution of this structure.

In this letter we are reporting a study of the space–time structure of magnetic fields in a laser plasma by a Faraday-effect method (a method based on the rotation of the polarization plane of a probe electromagnetic wave) and three-channel "polarinterferometry."[5] The diagnostic method is based on simultaneous measurements of the angle though which the polarization plane is rotated, $\alpha \propto \int Bn_e dl$, and the phase shift $\delta \propto \int n_e dl$ (B is the magnetic induction, n_e the electron density, and l the path length of the probe light in the plasma). The ratio of these integrals gives us the average magnetic field along the optical path. For an axisymmetric plasma, it is possible to reconstruct the local distributions $B(r)$ and $n_e(r)$ through an Abel transformation.[5]

For this study of the space–time distribution of the magnetic fields we assembled a diagnostic complex[6] for measuring magnetic fields both in the framing mode (with an exposure time ~ 1.5 ns) and in a dynamic mode (in this case we used two image-converter cameras operated in the streak mode). This complex simultaneously recorded Faraday-effect, shadow, and interference images of the plasma with a high spatial resolution, ~ 5 μm, and a high time resolution, ~ 50 ps. The contrast of the polarimeter was $\sim 3\times 10^{-5}$, so it was possible to measure the angle through which the polarization plane rotated within $\pm 0.1°$. The error in the determination of the phase

shift of the probe wave was ± 0.1 of a line. We used RF-3 photographic film, calibrated beforehand, for the recordings. The basic layout of the three-channel polarinterferometer is given in Ref. 7. The coordinate scales on the images were reconciled by means of a visualizing diaphragm in an intermediate image of the plasma.

To reconstruct the angle through which the polarization plane of the probe light was rotated, we carried out a two-dimensional digitalization of the Faraday-effect and shadow images of the plasma, using an AMD-1 microdensitometer controlled by a personal computer. Using a special computer program for working with two-dimensional data files, we then reconstructed pairs of corresponding radial profiles of the blackening on the Faraday-effect and shadow images. These profiles were then used to determine the angle through which the polarization plane was rotated, by the method of Ref. 5.

The experiments were carried out at the Feniks high-power single-beam Nd laser[8] with a wavelength of 0.527 μm, a pulse length ~ 1.5 ns, and an energy $\leqslant 10$ J. The intensity in the focus was $\leqslant 10^{15}$ W/cm^2. The pump light was focused on the surface of a plane Al target in a spot ~ 15 μm in diameter by means of a two-component objective with an aperture ratio 1:6. The probe light was light tapped from the pump beam and then frequency-doubled in a KDP crystal.

Figure 1a shows Faraday-effect (F_k), shadow (S_k), and interference (I_k) images of the laser plasma recorded in the framing mode 1 ns after the arrival of the peak of the pump pulse. The laser energy was $E=5.5$ J. The angle between the transmission axes of the polarizer and the analyzer differed from a right angle by an amount $\alpha_0=3°$ (the "decrossing" angle). On the Faraday-effect image of the plasma, in contrast with the shadow image, we can see a modulation of the light intensity due to differences in the direction of the angle (α) through which the polarization plane is rotated with respect to the axis of the pump light.

Figure 1b shows Faraday-effect (F_t), shadow (T_t), and interference (I_t) images of the laser plasma recorded by the image-converter cameras operating in the streak mode, at a distance $z=120$ μm from the target surface. The plasma was probed at the same time the pump light was incident; the laser energy was $E=2.5$ J, and the decrossing angle $\alpha_0=3°$. The Faraday-effect image, in contrast with the shadow image, has a modulation of the light intensity similar to that in Fig. 1a.

Under the assumption of an axial symmetry of the plasma we reconstructed local distributions of the magnetic induction and the electron density. Figure 2 shows the spatial–distribution $B(r,z)$ (Fig. 2a) and the spatial-temporal distribution $B(r,t)$ (Fig. 2b) corresponding to the images of the plasma in Fig. 1. The maximum magnetic field is $B_{\max}=400$ kG$\pm 20\%$ at a distance $z=115$ μm from the target surface, where the electron density is $n_e \sim 10^{20}$ cm^{-3}. The current density reaches ~ 90 mA/cm^2 at the axis of the pump beam. The maximum current flowing through the plasma in this region is ~ 24 kA.

Figure 3a shows the magnetic-field energy $E_B=\int (B^2/8\pi)dV$ (in the volume bounded by the cross sections $z_1=115$ μm and $z_2=175$ μm) versus the laser energy E. This energy increases essentially linearly with increasing laser energy; the ratio

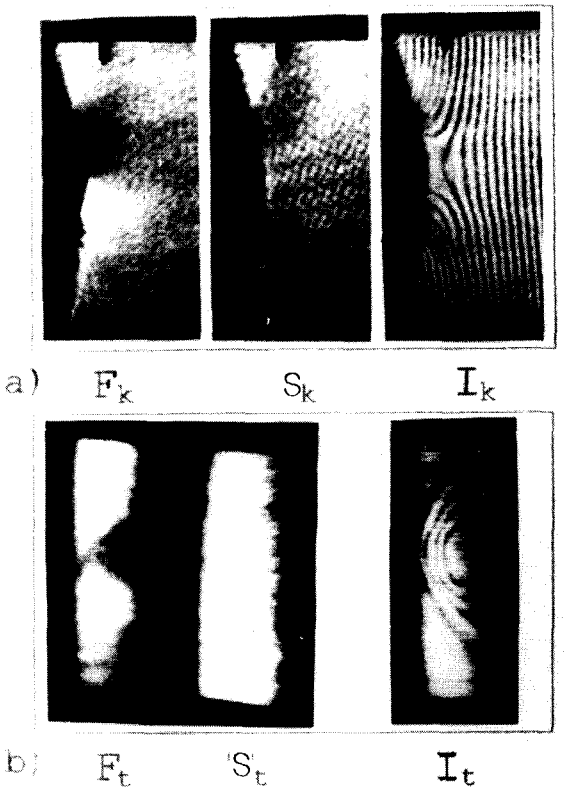

FIG. 1. Faraday-effect (F), shadow (S), and interference (I) images of a laser plasma. a—Recorded in framing mode; b—in streak-camera mode, with the help of image-converter cameras.

E_B/E is $\sim 1\%$. The ratio of the magnetic energy to the thermal energy $E_T = \int (n_e T_e) dV$ (at $T_e \approx 500$ eV) is $\sim 4\%$, independent of E.

Figure 3b shows the time evolution of the magnetic energy $E_B(t)$, the thermal energy of the plasma, $E_T(t)$, and the shape of the pump pulse, $I(t)$. We see that the changes in the magnetic energy correlate with the shape of the pump pulse. During the first half of the pulse, the magnetic energy E_B increases at a rate ~ 0.5 mJ/ns. During the second half of the pulse, E_B stops increasing and then decreases at a rate ~ 0.3 mJ/ns. At the same time, there is an essentially linear increase in the thermal energy of the plasma during the pump pulse, at a rate ~ 10 mJ/ns.

Several mechanisms are known to generate quasisteady magnetic fields in a laser plasma.[9] The experimental data can be explained by invoking two of them. The magnetic fields outside the laser beam, at distances $r \sim 50$–200 μm from the axis, could be generated only by a thermal-emf mechanism which arises because the gradients of the temperature and electron density are not collinear.[1,10] This mechanism is described by a source

$$S = S_T = \frac{c}{e n_e} \frac{\partial n_e}{\partial z} \frac{\partial T_e}{\partial r}. \qquad (1)$$

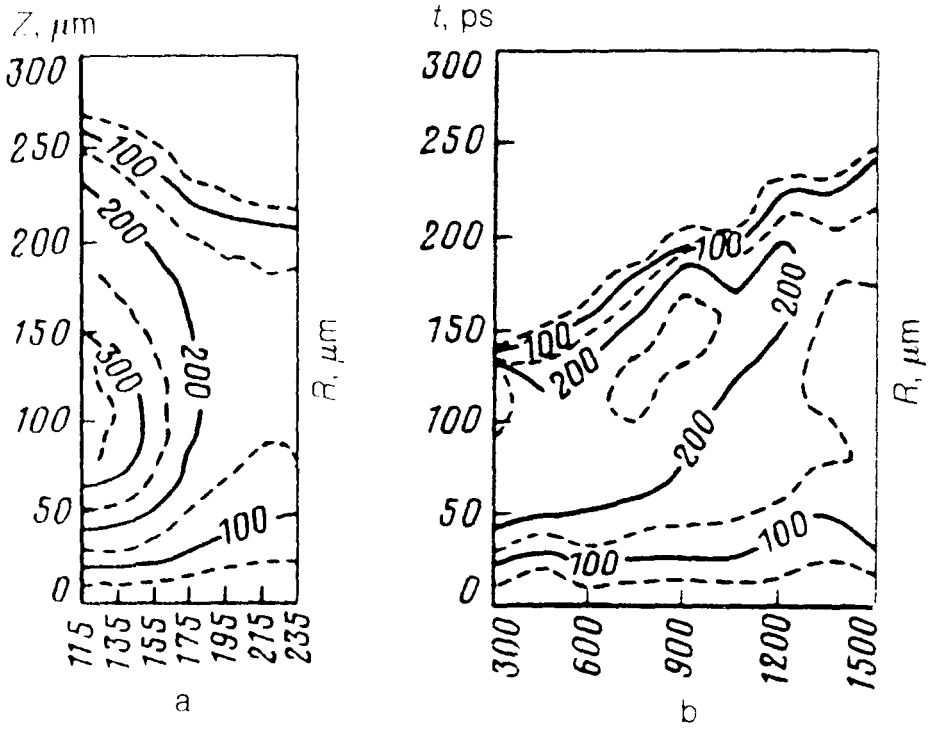

FIG. 2. Spatial (a) and spatial–temporal (b) structure of the magnetic field. The contour curves are spaced at $\Delta B = 50$ kG.

On the other hand, the thermal-emf mechanism cannot explain the peak in the current density at the axis of the pump beam, the temporal correlation of the magnetic energy and the energy of the laser pulse, or the substantial magnetic fields near the axis, at $r \sim 10$–$50\ \mu$m, in a region whose size is on the order of the diameter of the focus. These effects are apparently due to a ponderomotive emf [11] which arises because the gradients of the laser beam intensity and the plasma density are not collinear:[12]

$$S = S_E = -1.6 \frac{Z}{en_e n_c} \frac{\partial n_e}{\partial z} \frac{\partial I}{\partial r}, \tag{2}$$

where n_c is the critical electron density, $I = cE^2/8\pi$ is the intensity of the laser beam, and Z is the charge of the ion.

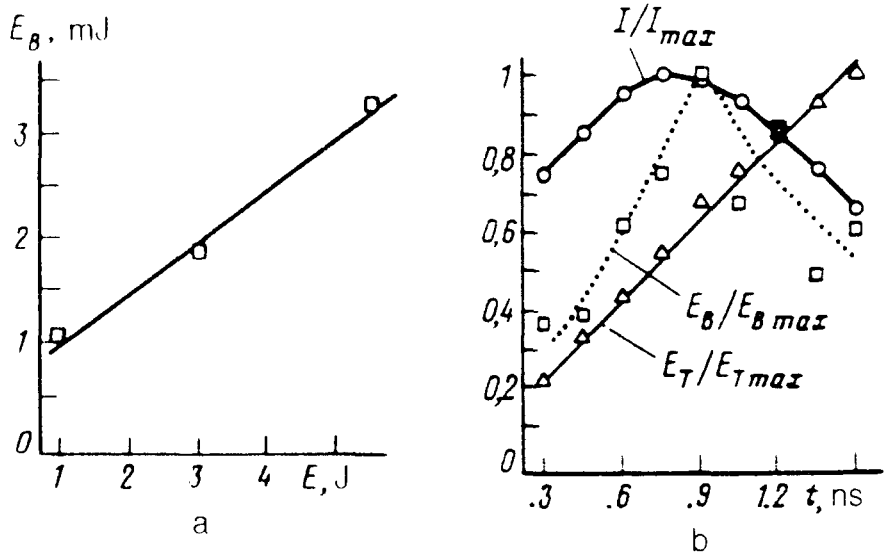

FIG. 3. a—Magnetic-field energy E_B versus the laser energy E; b— dynamics of the magnetic-field energy, $E_B(t)$, the thermal energy of the plasma, $E_T(t)$, and the shape of the pump pulse, $I(t)$ ($E_{B\max}=0.4$ mJ, $E_{T\max}=13$ mJ).

In principle, a current of fast electrons could also contribute to the generation of magnetic fields near the axis. However, the generation of fast electrons is a pulsed process,[8] while the magnetic induction varies quite smoothly during the laser pulse (Figs. 2b and 3b).

The magnitude of the source S characterizes the initial rate of increase of the magnetic field: $S=\dot{B}=\partial B/\partial t$. For the experimental conditions [$T_e\sim 0.5$ keV, $L_N=n/(\partial n/\partial z)\sim 100$ μm, $R_T=T_e/(\partial T_e/\partial z)\sim 200$ μm, $R_E=I/(\partial I/\partial z)\sim 10$ μm, $I\sim 3\times 10^{14}$ W/cm^2, $Z\sim 10$, and $n_e\sim 10^{20}$ cm^{-3}], expression (1) yields $S_T\sim 0.25$ MG/ns for the rate of increase of the magnetic field, while we have $S_E\sim 2.5$ MG/ns^2. The higher rate of increase which follows from (2) is a consequence of the small size of the focus, $R_E/R_T\ll 1$.

The magnetic field stops increasing with time and reaches a quasisteady level, as the result of transport out of the generation region by convection or diffusion. At distance scales $r\geqslant 100$ μm the rate of magnetic-field diffusion is about an order of magnitude lower than the expansion velocity $u_r\geqslant 2\times 10^7$ cm/s, although the two may be comparable near the axis. The quasisteady level of the magnetic field can thus be estimated from the balance between the rate at which the field is carried off and the rate at which it is generated:

$$\frac{\partial}{\partial r} u_r B \approx S_E + S_T. \tag{3}$$

In quasisteady state (3), the relative roles of mechanisms (1) and (2) change slightly. Although source S_E leads to a more rapid increase in the field, saturation occurs at approximately the same level as in the case in which the effect is caused by the thermal emf:

$$B_T \sim \frac{c}{e} \frac{T_e}{L_N u_r} = 250 \text{ kG}, \quad B_E \sim 1.6 \frac{Z}{en_c} \frac{I}{L_N u_r} = 100 \text{ kG}. \tag{4}$$

These results agree with the experimental data. The ponderomotive emf is responsible for the magnetic fields near the axis (at $r \leqslant 50$ μm), while the fields at the periphery ($r \geqslant 100$ μm) are due to the thermal emf. In the intermediate region, the two fields add together. The increase in the magnetic energy with the laser energy observed experimentally (Fig. 3a) is apparently due to both an increase in the fraction of the magnetic energy which is caused by the ponderomotive emf and an increase in the plasma volume. The experimental observation of a temporal correlation between the magnetic energy and the energy of pump light also indicates that the ponderomotive emf is playing an important role (Fig. 3b).

The magnetic fields observed experimentally should have a strong effect on transport in the plasma corona, since the electron cyclotron frequency is several times the electron collision rate. For this reason, the radial and axial heat fluxes are significantly suppressed, and the transport of plasma energy is apparently a convective removal. We should also take into account the large gradients, $\sim (20\ \mu\text{m})^{-1}$, observed experimentally in the magnetic field in the regions $r \leqslant 50$ μm and $r \geqslant 100$ μm. These large gradients are evidence of strong electric fields in these regions. These electric fields may cause a substantial acceleration of plasma in the radial direction through the Ampère force $c^{-1}[\mathbf{j} \times \mathbf{B}]$. In these regions, this force reaches $\sim 30\%$ of the thermal-pressure force. The magnetic field which is generated thus also has a strong effect on the hydrodynamics of the plasma. In the central region of the plasma, the plasma may be slowed by the Ampère force, while at the periphery it may be accelerated. This process may in turn affect the strength of the magnetic field and its spatial distribution.

[1] J. A. Stamper *et al.*, Phys Rev. Lett. **26**, 1012 (1971).
[2] J. A. Stamper and B. H. Ripin, Phys. Lett. **34**, 138 (1975).
[3] A. Raven, O. Willy, and P. T. Rumsby, Phys. Rev. Lett. **41**, 554 (1978).
[4] M. D. J. Burgess, B. Luther-Davies, and K. A. Nugent, Phys. Fluids **28**, 2286 (1985).

[5] T. Pisarchik, A. A. Rupasov, G. S. Sarkisov, and A. S. Shikanov, Preprint 135, P. N. Lebedev Physics Institute, Academy of Sciences of the USSR, Moscow, 1989; J. Sov. Laser Res. **11**, 1 (1990).
[6] Yu. S. Kas'yanov and G. S. Sarkisov, Preprint, P. N. Lebedev Physics Institute, Academy of Sciences of the USSR, Moscow, 1993.
[7] Z. Patron, T. Pisarchik, A. A. Rupasov *et al.*, Prib. Tekh. Eksp., No 1, 183 (1990).
[8] N. E. Andreev, V. L. Artsimovich, Yu. S. Kas'yanov, and V. T. Tikhonchuk, Zh. Eksp. Teor. Fiz. **98**, 881 (1990) [Sov. Phys. JETP **71**, 490 (1990)].
[9] M. G. Haines, Can. J. Phys. **64**, 912 (1986).
[10] D. A. Tidman and R. A. Shanny, Phys. Fluids **17**, 1207 (1974).
[11] V. I. Perel' and Ya. M. Pinskiĭ, Zh. Eksp. Teor. Fiz. **54**, 1889 (1969) [Sov. Phys. JETP **27**, 1014 (1968)].
[12] K. N. Ovchinnikov, V. P. Silin, and S. A. Uryupin, Fiz. Plazmy **17**, 1116 (1991) [Sov. J. Plasma Phys. **17**, 648 (1991)].

Translated by D. Parsons